Inorg. Chem. **2002**, *41*, 2408–2416

Photochemical Image Generation in a Cyanogel System Synthesized from Tetrachloropalladate(II) and the Trimetallic Mixed-Valence Complex $[(NC)_5Fe^{II}–CN–Pt^{IV}(NH_3)_4–NC–Fe^{II}(CN)_5]^{4-}$: Consideration of Photochemical and Dark Mechanistic Pathways of Prussian Blue Formation

David F. Watson, Jennifer L. Willson, and Andrew B. Bocarsly*

Department of Chemistry, Princeton University, Washington Road, Princeton, New Jersey 08544

Received July 5, 2001

The cyanogel system involving $PdCl_4^{2-}$ and the mixed-valence complex $[(NC)_5Fe^{II}–CN–Pt^{IV}(NH_3)_4–NC–Fe^{II}(CN)_5]^{4-}$ is reported. The system has been characterized by UV–vis absorption, diffuse reflectance infrared, and resonance Raman spectroscopies. Gelation occurs through coordination of Pd(II) to the nitrogen atom of terminal cyanide ligands in the mixed-valence complex. Irradiation into the Fe(II) → Pt(IV) intervalent electron transfer (IT) band of $[(NC)_5Fe^{II}–CN–Pt^{IV}(NH_3)_4–NC–Fe^{II}(CN)_5]^{4-}$ results in the formation of a variety of Prussian-blue-like species within the rigid cyanogel matrix. Photochemical and dark mechanisms involving coupled cyanide loss and Fe(II) oxidation are proposed for the formation of Prussian-blue-like species. The optical contrast between irradiated and nonirradiated regions of the gel enables photochemical image generation with at least 12 μm resolution. This capability is demonstrated through the production of a series of diffraction gratings in cyanogel samples.

Introduction

Our lab has extensively characterized the trimetallic, mixed-valence anion $[(NC)_5Fe^{II}–CN–Pt^{IV}(NH_3)_4–NC–Fe^{II}(CN)_5]^{4-}$ (herein referred to as Fe(II)−Pt(IV)−Fe(II)).[1–5] The visible absorption spectrum of this complex exhibits an intense band ($\epsilon = 2365\ M^{-1}\ cm^{-1}$) centered at 424 nm, corresponding to a photoinduced Fe(II) → Pt(IV) intervalent electron transfer (IT) absorption. Irradiation into this band leads to the dissociation of the complex into 2 equiv of $Fe(CN)_6^{3-}$ and 1 equiv of $Pt(NH_3)_4^{2+}$, which is a net two-electron-transfer process.[1] When Fe(II)−Pt(IV)−Fe(II) and its photoproducts are confined in a rigid matrix, photochemical image generation becomes possible. Our lab has produced images on indium tin oxide (ITO) electrodes, surface-modified with polymerized Fe(II)−Pt(IV)−Fe(II).[6,7] Irradiation of the surface-modified electrodes in $Fe(NH_3)_4(SO_4)$ solution resulted in the formation of Prussian blue on the ITO surface by the reaction of Fe^{2+} and the photochemically produced $Fe(CN)_6^{3-}$. The ability to generate images results from the differences in the Prussian blue and Fe(II)−Pt(IV)−Fe(II) absorption spectra and the resulting optical contrast between irradiated and nonirradiated portions of the electrode. By irradiating through a mask, arbitrary image generation was demonstrated with a scale on the order of 1 μm.[6,7]

In this paper, we report on the photochemical patterning of a rigid sol−gel generated matrix incorporating Fe(II)−Pt(IV)−Fe(II). Our lab has previously reported the synthesis of a series of hydrogel systems consisting of transition metal coordination polymers involving $PdCl_4^{2-}$ and $M(CN)_y^{x-}$, where M is a transition metal and $y = 4$, 6, or 8 depending on the metal employed.[8–10] In these "cyanogel" systems,

* To whom correspondence should be addressed. E-mail: bocarsly@princeton.edu.

(1) Zhou, M.; Pfennig, B. W.; Steiger, J.; Van Engen, D.; Bocarsly, A. B. *Inorg. Chem.* **1990**, *29*, 2456−2460.
(2) Pfennig, B. W.; Bocarsly, A. B. *Coord. Chem. Rev.* **1991**, *111*, 91−96.
(3) Pfennig, B. W.; Bocarsly, A. B. *J. Phys. Chem.* **1992**, *96*, 226−233.
(4) Pfennig, B. W.; Wu, Y.; Kumble, R.; Spiro, T. G.; Bocarsly, A. B. *J. Phys. Chem.* **1996**, *100*, 5745−5750.
(5) Wu, Y.; Pfennig, B. W.; Sharp, S. L.; Ludwig, D. R.; Warren, C. J.; Vicenzi, E. P.; Bocarsly, A. B. *Coord. Chem. Rev.* **1997**, *159*, 245−255.
(6) Wu, Y.; Pfennig, B. W.; Bocarsly, A. B. *Inorg. Chem.* **1995**, *34*, 4262−4267.
(7) Bocarsly, A. B.; Chang, C. C.; Wu, Y.; Vicenzi, E. P. *J. Chem. Educ.* **1997**, *74*, 663−667.
(8) Pfennig, B. W.; Bocarsly, A. B.; Prud'homme, R. B. *J. Am. Chem. Soc.* **1993**, *115*, 2661−2665.

10.1021/ic010710l CCC: $22.00
Published on Web 04/10/2002

aqueous solutions of $PdCl_4^{2-}$ and $M(CN)_y^{x-}$ react to form gelled polymeric materials containing bridging cyanide ligands between the Pd and M centers and typically containing ~95% water by weight. Of particular relevance to this study is the system involving $Fe(CN)_6^{4-}$ and $PdCl_4^{2-}$.[8] Because Fe(II)−Pt(IV)−Fe(II) contains two terminal $Fe(CN)_6^{4-}$ units, it is expected to form a cyanogel material when reacted with aqueous $PdCl_4^{2-}$. By locking the photoproducts of Fe(II)−Pt(IV)−Fe(II) in a rigid sol−gel matrix, image generation should be possible, because Fe(II)−Pt(IV)−Fe(II) and its photoproducts absorb in different regions of the visible spectrum.

A sol−gel photochemical image generation system has an inherent advantage over one in which the photochemically active species is deposited from solution onto the surface of a solid matrix. The initial liquid state of the sol−gel system enables unlimited control of sample size and shape. A number of silica and titania based sol−gel systems capable of photoinduced alteration of surface structure have been reported.[11−16] These systems typically consist of a tetravalent sol−gel backbone modified with photoactive substituents. The surface alteration mechanism usually involves the photoinduced polymerization or degradation of material, followed by a postphotochemical washing step.[16] The photoinduced steps generally require UV light. Several systems have been reported in which Bragg diffraction gratings are produced based on the photochemical alteration of the surface structure of the gel.[11,14−16]

The photochemistry of the cyanogel system herein reported offers the potential for image generation based on optical changes rather than changes in surface morphology. Optical pattern generation is potentially advantageous because postphotochemical treatment of the system is unnecessary. In addition, the cyanogel system offers the potential for photochemical patterning with visible instead of UV irradiation.

Experimental Section

Materials and Apparatus. $Pt(NH_3)_4(NO_3)_2$ was purchased from Aldrich. $K_3Fe(CN)_6$ was purchased from Fisher. Na_2PdCl_4 was purchased from Pressure Chemical Co. All reagents were used without further purification. Amberlite IR-120 sodium exchange column resin was obtained from Aldrich. Bio-Gel P-2 size exclusion column resin was obtained from Bio-Rad. UV−vis absorption spectra were obtained with a Hewlett-Packard HP8453 diode array spectrophotometer with 2 nm resolution. Diffuse reflectance Fourier transform infrared (FTIR) spectra were obtained as the average of 128 scans using a Nicolet 730 FTIR spectrometer with 4 cm^{-1} resolution. Cyclic voltammetry was performed using a Princeton Applied Research Model 263 potentiostat and a standard 3-electrode, single compartment electrochemical cell with an SCE reference electrode, an ITO working electrode, and a Pt counter electrode.

Synthesis of $Na_4[(NC)_5Fe^{II}-CN-Pt^{IV}(NH_3)_4-NC-Fe^{II}(CN)_5]$. The sodium salt of Fe(II)−Pt(IV)−Fe(II) was synthesized following the method of Chang et al.[17] $K_3Fe(CN)_6$ (0.400 g, 1.20 mmol) and $Pt(NH_3)_4(NO_3)_2$ (0.200 g, 0.520 mmol) were each dissolved in 5.0 mL of deionized H_2O. Under subdued lighting, the $Pt(NH_3)_4(NO_3)_2$ solution was added dropwise to the $K_3Fe(CN)_6$ solution, at room temperature with stirring. The resulting deep red solution was first run through an Amberlite IR-120 sodium exchange column charged with 1.0 M NaCl solution, then through a Bio-Gel P-2 size exclusion column. The product was collected in fractions, which were analyzed for $Fe(CN)_6^{3-}$ impurity by cyclic voltammetry. Fractions which exhibited measurable ferri/ferrocyanide redox waves were rejected. Pure fractions were combined and air-dried in the dark, yielding the desired product.

Synthesis of [Fe(II)−Pt(IV)−Fe(II)]−[$PdCl_4^{2-}$] Cyanogel Samples. Aqueous solutions of Na_4[Fe(II)−Pt(IV)−Fe(II)] (50 mM) and Na_2PdCl_4 (50 mM) were combined in a 1:4 (v/v) ratio. Within 10 min, the samples formed a rigid cyanogel network. The pH of these samples was 3.0. Samples at pH 3.4 were prepared by dissolving Na_4[Fe(II)−Pt(IV)−Fe(II)] and Na_2PdCl_4 in 0.1 M pH 4.0 $KHC_8H_4O_4$ buffer. Samples at pH 4.9 were prepared by dissolving Na_4[Fe(II)−Pt(IV)−Fe(II)] and Na_2PdCl_4 in 0.1 M pH 5.9 KH_2PO_4 buffer. Samples at pH 5.5 were prepared by dissolving Na_4[Fe(II)−Pt(IV)−Fe(II)] and Na_2PdCl_4 in 0.1 M pH 7.0 KH_2PO_4 buffer. Samples at pH 6.0 were prepared by dissolving Na_4[Fe(II)−Pt(IV)−Fe(II)] and Na_2PdCl_4 in 0.1 M pH 8.1 KH_2PO_4 buffer. Samples at pH 7.0 were prepared by dissolving Na_4[Fe(II)−Pt(IV)−Fe(II)] and Na_2PdCl_4 in 0.05 M pH 10.0 $NaHCO_3$ buffer. In sample preparation under Ar or O_2 atmosphere, deionized H_2O was purged for 15 min with the appropriate gas. A glovebag was sealed and purged with the appropriate atmosphere for 60 min. Samples were prepared as described previously, and photochemical cells were sealed with epoxy (as described later) prior to removal from the glovebag.

Resonance Raman Spectroscopy. Samples were prepared as described previously and transferred to NMR tubes prior to gelation. Resonance Raman spectra were collected in a 135° backscattering geometry with a Spex 1877 triple monochromator equipped with a Princeton Instruments intensified diode array detection system. Observed spectra were calibrated using the known frequencies of the DMSO-d_6 spectrum obtained under identical optical alignment as that of the sample. Laser excitation at 482.5 nm, 60 mW was provided by a Spectra-Physics BeamLok 2080-RS3 Kr^+ ion laser.

Photochemistry. Sample containers with 0.12 and 0.03 cm path lengths were used in photochemical studies. The 0.12 cm cells consisted of 0.015 cm thick glass windows (VWR No. 1 microscope cover slips) separated by 0.12 cm thick glass spacers (VWR microscope slides). The 0.03 cm cells consisted of 0.015 cm thick glass windows separated by two 0.015 cm thick glass spacers. Prior to sample addition, three sides of the sample cell were sealed with a thin layer of epoxy. Cyanogel samples were mixed in a separate

(9) Heibel, M.; Kumar, G.; Wyse, C.; Bukovec, P.; Bocarsly, A. B. *Chem. Mater.* **1996**, *8*, 1504−1511.
(10) Sharp, S. L.; Bocarsly, A. B.; Scherer, G. W. *Chem. Mater.* **1998**, *10*, 825−833.
(11) Krug, H.; Schmidt, H. *New J. Chem.* **1994**, *18*, 1125−1134.
(12) Andrews, M. P.; Najafi, S. I. In *Sol−Gel and Polymer Photonic Devices: Critical Reviews of Optical Sciences and Technology*; Andrews, M. P., Najafi, S. I., Eds.; SPIE: Bellingham, WA, 1997; Vol. CR68, pp 253−285.
(13) Moureau, Y.; Arguel, P.; Coudray, P.; Porque, J.; Etienne, P. In *Integrated Optic Devices II, SPIE Proc. 38*; Righini, G. G., Najafi, S. I., Jalali, B., Eds.; SPIE: Bellingham, WA, 1998; pp 179−186.
(14) Rantala, J. T.; Äyräs, P.; Levy, R.; Honkanen, S.; Descour, M. R.; Peyghambarian, N. *Opt. Lett.* **1998**, *23*, 1939−1941.
(15) Äyräs, P.; Rantala, J. T.; Honkanen, S.; Mendes, S. B.; Peyghambarian, N. *Opt. Commun.* **1999**, *162*, 215−218.
(16) Blanc, D.; Pelissier, S.; Saravanamuttu, K.; Najafi, S. I. *Adv. Mater.* (*Weinheim, Ger.*) **1999**, *11*, 1508−1511.
(17) Chang, C.; Ludwig, D.; Bocarsly, A. B. *Inorg. Chem.* **1998**, *37*, 5467−5473.

glass vial and then transferred into the photochemical cells through the unsealed side of the cell prior to sample gelation. After gelation, the fourth side of the cell was sealed with epoxy in order to avoid concentration of the samples through evaporation. The samples were irradiated at 488.0 nm with an expanded beam (1.0 cm diameter) from a Coherent Innova 70 Ar^+ ion laser. Typical light intensity was 50−150 mW/cm^2.

Photochemical Image Generation. Samples in 0.12 cm path length photochemical cells were placed horizontally on a laser table. The samples were irradiated for 12−16 h at 488.0 nm, 90 mW/cm^2 with a 1.0 cm diameter beam, through a diffraction grating mask which was placed directly on top of the cyanogel sample. The diffraction grating mask was either the "Unit Cell Slide" or the "Discovery Slide" from the Institute for Chemical Education's *Optical Transform Kit*.[18] The samples were irradiated through regions A−D of the slide. Optical microscopy was performed using a Wild Heerbrugg microscope. Diffraction patterns were generated by shining 680 nm light from a diode laser or 633 nm light from a He−Ne laser through the patterned cyanogel sample. Intensity of diffracted light was measured using a ThorLabs, Inc. DET210 silicon photodiode output to a Houston Instruments model 2000 X-Y recorder.

Results and Discussion

Structural Characterization. When aqueous solutions of Fe(II)−Pt(IV)−Fe(II) and $PdCl_4^{2-}$ were mixed, the intensity of dark orange coloration of the sample increased, concomitant with an increase in solution viscosity. The mixture typically gelled within 5 min. When 10 mM or greater concentrations were used, the sample container could be inverted without disturbing the gel network. The physical appearance of the gel resembled that of previously reported $[M(CN)_y^{x-}]-[PdCl_4^{2-}]$ cyanogel systems.[8] The [Fe(II)−Pt(IV)−Fe(II)]−$[PdCl_4^{2-}]$ samples were stable at room temperature for up to several weeks. Eventually, they turned green but remained in the gelled state. The UV−vis absorption spectrum of [Fe(II)−Pt(IV)−Fe(II)]−$[PdCl_4^{2-}]$ cyanogel samples contains a broad new absorption band centered at 342 nm (Figure 1). The new band overlaps with the high-energy region of the Fe(II)−Pt(IV)−Fe(II) IT band centered at 422 nm. We have assigned the new absorption as Fe(II) → Pd(II) IT. A Job plot[19] of the absorbance at 350 nm versus mole fraction $PdCl_4^{2-}$ indicates that Fe(II)−Pt(IV)−Fe(II) and $PdCl_4^{2-}$ combine to form a product with 1:4 stoichiometry (Figure 1 inset). Our lab has previously proposed a star polymer structure for $[M(CN)_y^{x-}]-[PdCl_4^{2-}]$ cyanogel systems, in which the molar ratio of $M(CN)_y^{x-}$ to $PdCl_4^{2-}$ is 1:2.[8,10] Because Fe(II)−Pt(IV)−Fe(II) contains two terminal ferrocyanide units, the observed 1:4 Fe(II)−Pt(IV)−Fe(II) to $PdCl_4^{2-}$ molar ratio suggests that a similar structure is adopted in the [Fe(II)−Pt(IV)−Fe(II)]−$[PdCl_4^{2-}]$ cyanogel system. The proposed structure is shown in Figure 2. On the basis of the calculated optimum molar ratio, all samples prepared for further characterization and photochemical studies consisted of 1:4 (v/v) 50 mM Na_4[Fe(II)−Pt(IV)−Fe(II)](aq)/50 mM Na_2PdCl_4(aq). These samples were acidic (pH 3.0), because of the hydrolysis of $PdCl_4^{2-}$.

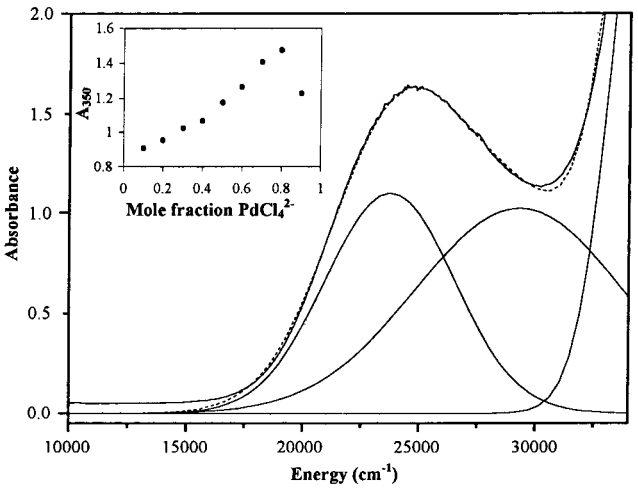

Figure 1. UV−vis absorption spectrum of [Fe(II)−Pt(IV)−Fe(II)]−$[PdCl_4^{2-}]$ and a fit to three Gaussian bands. The observed absorption centered at 24700 cm^{-1} (405 nm) consists of bands with maxima at 29300 cm^{-1} (341 nm, Fe(II) → Pd(II) IT) and 23700 cm^{-1} (422 nm, Fe(II) → Pt(IV) IT). Dashed line shows the sum of component bands of the fit. Inset: Job plot of A_{350} versus mole fraction $PdCl_4^{2-}$ suggests 1:4 Fe(II)−Pt(IV)−Fe(II)/$PdCl_4^{2-}$ stoichiometry.

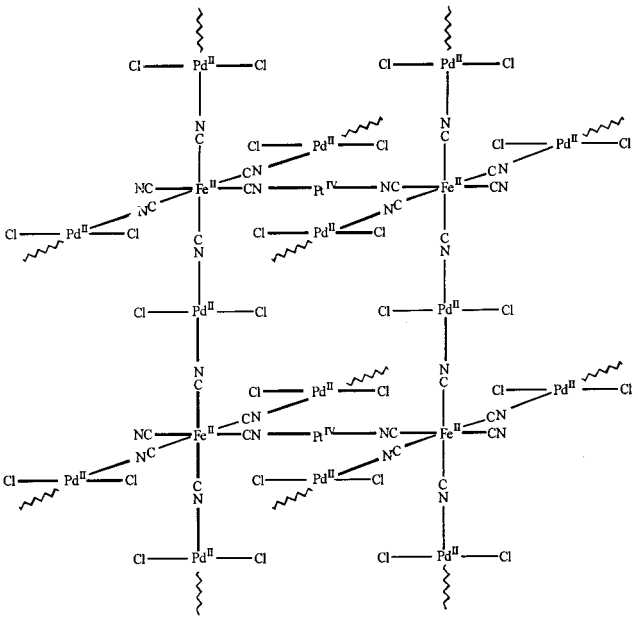

Figure 2. Proposed structure of the [Fe(II)−Pt(IV)−Fe(II)]−$[PdCl_4^{2-}]$ cyanogel system. Ammine ligands at Pt(IV) centers have been omitted for clarity. The experimentally determined 1:4 Fe(II)−Pt(IV)−Fe(II)/$PdCl_4^{2-}$ molar ratio suggests that polymerization occurs primarily through coordination of Pd(II) to radial terminal cyanide ligands of Fe(II)−Pt(IV)−Fe(II).

The diffuse reflectance FTIR spectrum of a [Fe(II)−Pt(IV)−Fe(II)]−$[PdCl_4^{2-}]$ xerogel sample, obtained by dehydrating a hydrogel sample at room temperature and pressure, contains a broad set of bands in the cyanide stretching region, with peaks at 2085 and 2135 cm^{-1} and a shoulder at 2205 cm^{-1}. The infrared spectrum of the polycrystalline $Pt(NH_3)_4^{2+}$ salt of Fe(II)−Pt(IV)−Fe(II) contains much narrower bands at 2055 and 2125 cm^{-1}, which were assigned as ν-CN(terminal) and ν-CN(Fe−Pt bridge), respectively.[1] By analogy, the bands at 2085 and 2135 cm^{-1}

(18) *Optical Transform Kit*: Available from Optical Transforms, Institute for Chemical Education, Department of Chemistry, University of Wisconsin−Madison, 1101 University Ave., Madison, WI, 53706.
(19) Vosburgh, W. C.; Cooper, G. R. *J. Am. Chem. Soc.* **1941**, *63*, 437−442.

in the infrared spectrum of [Fe(II)−Pt(IV)−Fe(II)]−[$PdCl_4^{2-}$] have been assigned as ν-CN(terminal) and ν-CN(Fe−Pt bridge), respectively. The increase in the frequencies of these bands is reasonable in light of the electron-withdrawing effect of the Pd(II) center. The presence of the Pd(II) center should cause a positive shift in the $Fe^{III/II}$ reduction potential,[1,8,9] or, equivalently, a decrease in the Fe t_{2g} orbital energies, which should in turn cause a reduction in the degree of Fe(t_{2g}) to CN(π*) back-bonding. The decrease in back-bonding strength should cause an increase in C−N bond strength and ν-CN frequency. The new band at 2205 cm^{-1} has been assigned as ν-CN(Fe−Pd bridge). The infrared spectrum of the [$Fe(CN)_6^{4-}$]−[$PdCl_4^{2-}$] cyanogel system was reported to have a ν-CN(Fe−Pd bridge) band at 2105 cm^{-1}.[20] The increase in the ν-CN(Fe−Pd bridge) frequency in the spectrum of [Fe(II)−Pt(IV)−Fe(II)]−[$PdCl_4^{2-}$] can be explained by the more positive $Fe^{III/II}$ reduction potential and resulting weaker Fe(t_{2g}) to CN(π*) back-bonding in Fe(II)−Pt(IV)−Fe(II) than in $Fe(CN)_6^{4-}$. The presence of a second bridging cyanide stretching band and the overall increase in bandwidth of the cyanide stretching region of the infrared spectrum provide strong evidence that coordination of cyanide to palladium is the mechanism of gelation, as in the proposed star polymer structure.

Photochemistry and Raman Spectroscopy. Prolonged irradiation of [Fe(II)−Pt(IV)−Fe(II)]−[$PdCl_4^{2-}$] cyanogel samples caused a noticeable change in coloration from orange to green in the irradiated region of the sample, corresponding to the growth of a broad absorption band extending from the low-energy tail of the IT bands to roughly 1000 nm. At the same time, the absorbance in the low-energy portion of the IT bands decreased significantly. The clear distinction in color between the irradiated and nonirradiated regions of the gel remained intact for up to several weeks. The absorption spectra of nonirradiated samples underwent similar changes, but on a much slower time scale (weeks).

The cyanide stretching region of the [Fe(II)−Pt(IV)−Fe(II)]−[$PdCl_4^{2-}$] resonance Raman spectrum was obtained with 482.5 nm incident irradiation. Initially, the spectrum consisted of bands at 2125, 2155, and 2205 cm^{-1}. These bands are assigned as ν-CN(terminal), ν-CN(Fe−Pt bridge), and ν-CN(Fe−Pd bridge), by analogy with the infrared spectrum of [Fe(II)−Pt(IV)−Fe(II)]−[$PdCl_4^{2-}$] and the previously reported Raman spectrum of aqueous Fe(II)−Pt-(IV)−Fe(II).[4] An additional band at 2218 cm^{-1} grew in very rapidly with irradiation of the sample during spectral acquisition. At the same time, the intensities of the 2125 and 2155 cm^{-1} bands decreased sharply. A noticeable region of green coloration developed in the irradiated area of the sample, corresponding to the growth of the red absorption band with irradiation. The evolution of the Raman spectrum with time is shown in Figure 3. The spectra are fairly noisy because they were obtained with relatively short integration times in order to obtain multiple spectra within the time scale of the spectral changes.

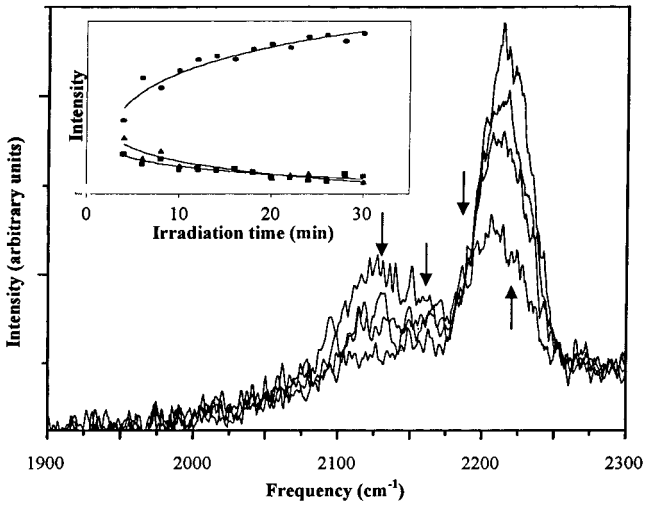

Figure 3. Cyanide stretching region of the resonance Raman spectrum of [Fe(II)−Pt(IV)−Fe(II)]−[$PdCl_4^{2-}$] with 482.5 nm, 60 mW incident irradiation. The spectra shown were obtained at 4, 6, 12, and 30 min total irradiation time. The evolution of the Raman spectrum is indicated by the arrows. Inset: intensity of the 2125 cm^{-1} (▲), 2155 cm^{-1} (■), and 2218 cm^{-1} (●) bands as a function of irradiation time.

The UV−vis and Raman spectral changes suggest that Prussian blue (PB) or PB-like species are formed with irradiation. It is well-known that $Fe(CN)_6^{3-}$ undergoes photoaquation in aqueous solution.[21,22] Thus, $Fe(CN)_6^{3-}$, which is formed through the photodissociation of Fe(II)−Pt(IV)−Fe(II), should further react to form $Fe(CN)_5(H_2O)^{2-}$, which could in turn react with Fe(II)−Pt(IV)−Fe(II) to form the mixed-valence species $[(NC)_5-Fe^{II}-CN-Pt^{IV}(NH_3)_4-NC-Fe^{II}(CN)_4-CN-Fe^{III}(CN)_5]^{6-}$. Like Prussian blue,[23,24] this complex contains an Fe(II) center coordinated to the carbon atom of the bridging cyanide ligand and an Fe(III) center coordinated to the nitrogen atom. Because the photochemically active species in the cyanogel system are part of a coordination polymer, any number of similar polymeric PB-like species may be formed, varying in the number of Fe(II)−Pt(IV)−Fe(II) subunits, the number of Pd(II) linkages, and the number of Fe(III) linkages. We refer to these PB-like species collectively as $PB^{▼}$.

The formation of these $PB^{▼}$ accounts for the observed changes in the UV−vis and Raman spectra of [Fe(II)−Pt(IV)−Fe(II)]−[$PdCl_4^{2-}$] upon irradiation. The band which develops in the red portion of the visible absorption spectrum corresponds to the Fe(II) → Fe(III) IT process which gives rise to the observed green coloration. The decrease of absorbance in the low energy region of the overlapping IT bands from 355 to 525 nm corresponds to the loss of the Fe(II) → Pt(IV) IT band upon photodissociation of Fe(II)−Pt(IV)−Fe(II). The 2218 cm^{-1} Raman band has been assigned as ν-CN(Fe(II)−Fe(III) bridge). The corresponding ν-CN(Fe(II)−Fe(III) bridge) frequency in PB is 2152 cm^{-1}.[25]

(20) Heibel, M. Sol−Gel Chemistry of the New Inorganic Polymers − Cyanogels. Ph.D. Thesis, University of Ljubljana, Ljubljana, Slovenia, 1996.

(21) Moggi, L.; Bolletta, F.; Balzani, V.; Scandola, F. *J. Inorg. Nucl. Chem.* **1966**, *28*, 2583−2597.
(22) Balzani, V.; Carassiti, V. *Photochemistry of Coordination Compounds*; Academic Press: New York, 1970.
(23) Duncan, J. F.; Wigley, P. W. R. *J. Chem. Soc.* **1963**, 1120−1125.
(24) Robin, M. B.; Day, P. *Adv. Inorg. Chem.* **1967**, *10*, 247−423.
(25) McCann, L. I.; Trentelman, K.; Possley, T.; Golding, B. *J. Raman Spectrosc.* **1999**, *30*, 121−132.

The greater frequency of this band in the PB▾ species presumably results from a positive shift of the $Fe^{III/II}$ reduction potential in PB▾ and subsequent decrease in $Fe(t_{2g})$ to $CN(\pi^*)$ back-bonding strength, due to the presence of the Pt(IV) and Pd(II) centers.[1,8,17] The disappearance of the 2125 cm^{-1} Raman band upon irradiation results from a decrease in the number of terminal Fe(II) cyanide ligands through both oxidation of terminal ferrocyanide units to ferricyanide upon dissociation of the complex and coordination of Fe(II)-bound terminal cyanide ligands to Fe(III) upon formation of PB▾. Similarly, the decreased intensity of the 2155 cm^{-1} Raman band results from a decrease in the number of Fe(II)−CN−Pt(IV) bridging cyanide sites upon photodissociation of the complex.

To lend support to the proposed photochemical formation of PB▾ in the cyanogel system, the PB-like species $[(NC)_5-Fe^{II}-CN-Pt^{IV}(NH_3)_4-NC-Fe^{II}(CN)_4-CN-Fe^{III}(CN)_5]^{6-}$ was synthesized in solution. Aqueous Fe(II)−Pt(IV)−Fe(II) and $FeCl_3$ were combined in a 1:1 molar ratio. The resulting mixture turned bluish green, because of the growth of a broad Fe(II) → Fe(III) absorption band centered at 680 nm. The infrared spectrum of this complex contained two bridging cyanide stretching bands, corresponding to the μ-[Fe(II)−Pt(IV)] and μ-[Fe(II)−Fe(III)] bridging cyanide ligands. The formation of this complex in solution provides strong evidence for the proposed formation of similar PB-like species in irradiated cyanogel samples.

The observed slow onset of green coloration in nonirradiated [Fe(II)−Pt(IV)−Fe(II)]−$[PdCl_4^{2-}]$ samples indicates that PB▾ formation may occur by a dark reaction mechanism as well as a photochemical mechanism. It has been shown that $Fe(CN)_6^{4-}$ is oxidized to Prussian blue in acidic solution.[26] Similarly, acid-catalyzed Fe(II)−Pt(IV)−Fe(II) oxidation could lead to PB▾ formation in the cyanogel system.

Elucidation of the Mechanism of PB▾ Formation. To confirm that both photochemical and dark pathways for PB▾ formation occur, a series of gel samples were irradiated at various intensities of 488 nm light. Plots of the change in absorbance at 450 and 675 nm versus time (A_{450} vs t and A_{675} vs t) and the change in absorbance at 450 and 675 nm versus number of incident photons are shown in Figure 4. (A_{450} is a measure of the loss of the Fe(II) → Pt(IV) IT band of Fe(II)−Pt(IV)−Fe(II), while A_{675} is a measure of the growth of the Fe(II) → Fe(III) IT band of PB▾.) In the A versus t plots for the irradiated samples (Figure 4a), the decrease of A_{450} and increase of A_{675} are intensity dependent, indicating that the observed spectral changes are due to a photochemical process. The nonirradiated sample also undergoes significant loss of A_{450} and growth of A_{675}, indicating that a dark reaction pathway leads to the observed absorbance changes, as well. The A versus t plots of the nonirradiated sample were subtracted from those of the irradiated samples, giving rise to the net A vs t plots in Figure 4b. The ratios of the initial slopes of the net A vs t plots correspond well with the ratios of light intensities, indicating that the dark reaction

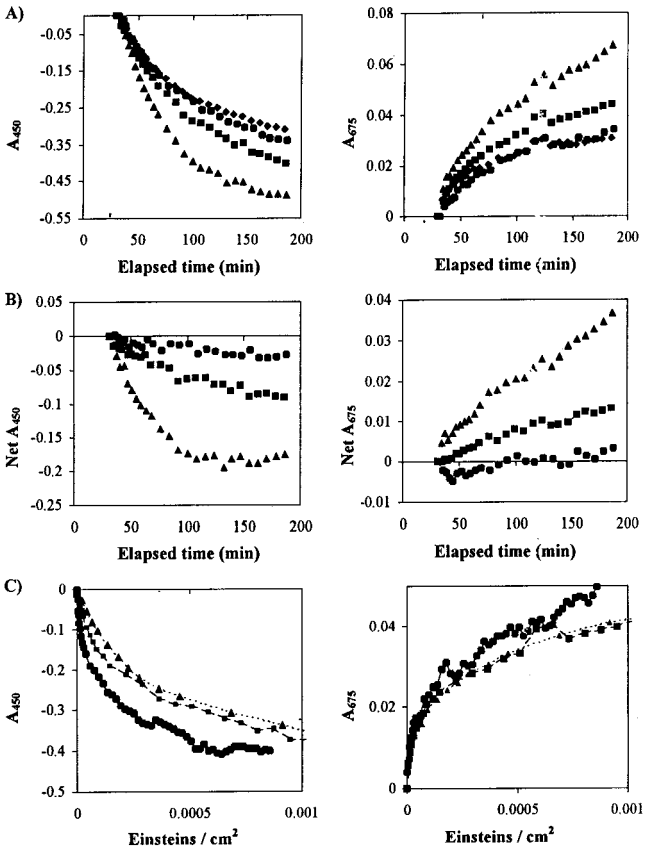

Figure 4. Intensity dependence of [Fe(II)−Pt(IV)−Fe(II)]−$[PdCl_4^{2-}]$ photochemistry. (A) Plots of A_{450} and A_{675} vs elapsed time. (B) Plots of net A_{450} and net A_{675} vs elapsed time. (C) Plots of A_{450} and A_{675} vs number of incident photons. (A_{450}, A_{675}, net A_{450}, and net A_{675} are defined in the text.) In all plots, ◆ = nonirradiated control sample; ● = 10 mW/cm^2 irradiated sample; ■ = 40 mW/cm^2 irradiated sample; ▲ = 120 mW/cm^2 irradiated sample. Samples were irradiated at 488 nm with a 1.0 cm diameter beam.

contribution to the absorbance changes in the irradiated samples is equal, regardless of irradiation intensity, and can be subtracted from the photochemical contribution.

In Figure 4c, which shows the variation of A versus the number of incident photons, the decrease of A_{450} and increase of A_{675} *per photon* are greatest with 10 mW/cm^2 irradiation and least with 120 mW/cm^2 irradiation. For the sample irradiated at 10 mW/cm^2, a greater amount of time elapses per incident photon than for the sample irradiated at 120 mW/cm^2. Thus, the contribution from the dark mechanism of PB▾ formation is greater per incident photon in the 10 mW/cm^2 sample than in the 120 mW/cm^2 sample, giving rise to greater absorbance changes in the A versus incident photon plots. This result further suggests that both dark and photochemical mechanisms for the formation of PB▾ exist and are totally independent of one another in the [Fe(II)−Pt(IV)−Fe(II)]−$[PdCl_4^{2-}]$ cyanogel system.

Cyanide loss and Fe(II) oxidation are the two main steps necessary for the formation of PB▾ from Fe(II)−Pt(IV)−Fe(II). A series of experiments was performed to investigate the roles of H^+, Pd^{2+}, and O_2 in the mechanism. In the first of these experiments, aqueous samples of Fe(II)−Pt(IV)−Fe(II) alone and Fe(II)−Pt(IV)−Fe(II) + $PdSO_4$ were irradiated at 488 nm. The solutions were buffered at pH 4.0. (Aqueous solutions of $PdSO_4$ and Fe(II)−Pt(IV)−Fe(II) did

(26) Baur, E. *Helv. Chim. Acta* **1925**, *8*, 403−405.

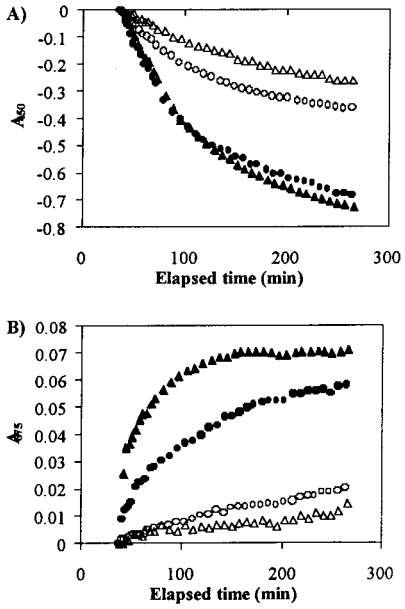

Figure 5. Plots of A_{450} and A_{675} vs t for [Fe(II)−Pt(IV)−Fe(II)]−[$PdCl_4^{2-}$] samples under Ar and O_2 atmospheres. In both plots, △ = nonirradiated Ar sample; ▲ = irradiated Ar sample; ○ = nonirradiated O_2 sample; ● = irradiated O_2 sample. Samples were irradiated at 488 nm, 90mW/cm^2 with a 1.0 cm diameter beam.

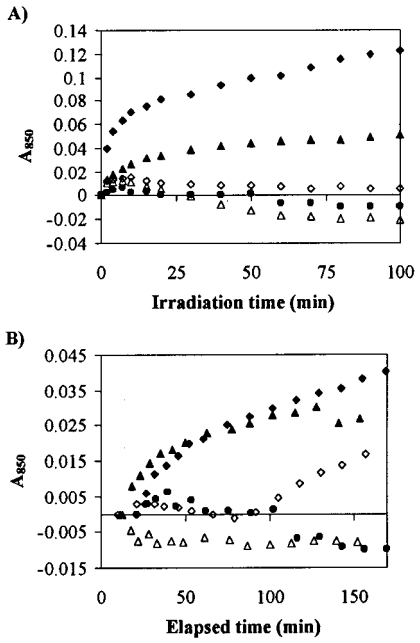

Figure 6. pH-dependence of [Fe(II)−Pt(IV)−Fe(II)]−[$PdCl_4^{2-}$] photochemistry. (A) Plot of A_{850} vs irradiation time for samples irradiated at 488 nm, 70 mW. (B) Plot of A_{850} vs elapsed time for nonirradiated samples. In both plots, ◆ = pH 3.0; □ = pH 3.4; ▲ = pH 4.9; ● = pH 5.5; △ = pH 6.0; and ◇ = pH 7.0. The apparent increase of A_{850} in the nonirradiated pH 7.0 sample after 100 minutes is artifactual, resulting from an increase in sample concentration due to evaporation.

not gel, consistent with previously reported [$PdCl_4^{2-}$]−[$M(CN)_y^{x-}$] cyanogel systems.)[8] Over the course of several hours, there was significant growth of an Fe(II) → Fe(III) IT band in both the irradiated and nonirradiated Fe(II)−Pt(IV)−Fe(II) + $PdSO_4$ samples. The absorbance increase was greater in the irradiated sample than in the nonirradiated sample, once again indicating that both dark and photochemical processes lead to the formation of PB▾. Significant growth of the Fe(II) → Fe(III) band was observed in the irradiated solution of Fe(II)−Pt(IV)−Fe(II) alone at pH 4.0. In the nonirradiated solution of Fe(II)−Pt(IV)−Fe(II) alone, neither a decrease of the Fe(II) → Pt(IV) band nor a growth of the Fe(II) → Fe(III) band was observed, indicating that PB▾ formation was negligible in the absence of Pd^{2+} at pH 4.0 in the aqueous sample. The results of this experiment suggest that Pd^{2+} enhances the rate of photochemical and dark PB▾ formation.

To investigate the role of O_2 in the PB▾ formation mechanism, samples of [Fe(II)−Pt(IV)−Fe(II)]−[$PdCl_4^{2-}$] were prepared and irradiated under Ar and O_2 atmospheres. Figure 5 shows A_{450} versus t and A_{675} versus t plots for nonirradiated and irradiated samples under Ar and O_2 atmospheres. The data clearly show that the increase of A_{675} and decrease of A_{450} occur more rapidly under O_2 than under Ar in the spectra of the nonirradiated samples. In the irradiated samples, there is little difference between the spectral changes of the samples under Ar and O_2 atmospheres.

The pH-dependence of PB▾ formation in the cyanogel system was studied by irradiating [Fe(II)−Pt(IV)−Fe(II)]−[$PdCl_4^{2-}$] samples prepared at different pHs. Plots of A_{850} versus t are shown in Figure 6a for irradiated samples at pH 3.0, 3.4, 4.9, 5.5, 6.0, and 7.0. (The change in absorbance at 850 nm is a measure of the Fe(II) → Fe(III) IT band growth of the PB▾ formed upon irradiation.) Figure 6a reveals that the Fe(II) → Fe(III) IT band grows in significantly faster during irradiation of the more acidic samples. At pHs of 5.5 and above, the Fe(II) → Fe(III) IT band did not grow in at all. Visibly, the irradiated region of the higher pH gels lost intensity of orange coloration (corresponding to the loss of the Fe(II) → Pt(IV) IT band) but did not turn green. The decrease in the Fe(II) → Pt(IV) IT absorbance at higher pHs indicates that the photodissociation of Fe(II)−Pt(IV)−Fe(II) and subsequent formation of $Fe(CN)_6^{3-}$ is pH-independent. Plots of A_{850} versus t for the corresponding nonirradiated control samples (Figure 6b) reveal that PB▾ formation is prohibited at higher pHs. It is also interesting to note that, at a given pH, the increase in A_{850} is significantly greater in the irradiated sample than in the nonirradiated sample, once again suggesting that independent photochemical and dark pathways exist for the formation of PB▾. The pH-dependence of PB▾ formation allows some degree of tunability of image formation. In acidic samples, the irradiated portion of the gel turns green, while in more basic samples the irradiatied portion of the gel turns pale yellow.

On the basis of the experiments to elucidate the roles of H^+, Pd^{2+}, and O_2, we have formulated a mechanism of PB▾ formation involving coupled cyanide loss and Fe(II) oxidation. The overall mechanism is shown in Scheme 1. First, we will consider the dark mechansim. In step 1a, H^+ ions undergo hydrogen bonding to the nitrogen atoms of terminal cyanide ligands. The electron withdrawing effect of the positively charged H^+ ions should lower the energy of the Fe(II) t_{2g} orbitals, thereby weakening the Fe(t_{2g}) to CN(π^*) back-bonding interaction and facilitating ligand loss (step 2a). The Pd(II) centers coordinated through cyanide to

Scheme 1. Proposed Mechanism of PB▼ Formation in the [Fe(II)−Pt(IV)−Fe(II)]−[$PdCl_4^{2-}$] Cyanogel System[a]

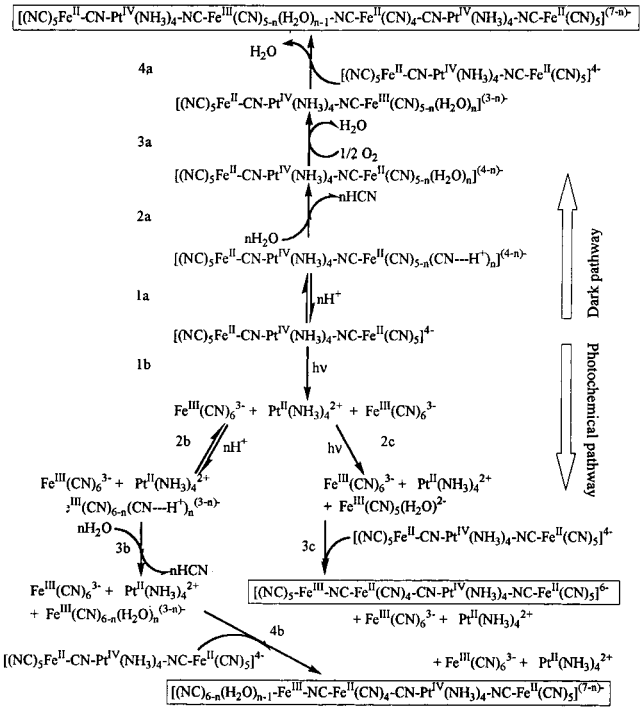

[a] $PdCl_4^{2-}$ has been omitted for clarity, because it is not photochemically active.

Fe(II) should enhance the electron withdrawing effect and further promote cyanide loss. Because H_2O is a weaker field ligand than cyanide, the $Fe^{III/II}$ redox potential of $[Fe^{II}(CN)_{6-n}(H_2O)_n]^{(4-n)-}$ centers within the cyanogel network should be more negative than that of $[Fe^{II}(CN)_6]^{4-}$ centers. Therefore, Fe(II) oxidation by O_2 should be more favorable in $[Fe^{II}(CN)_{6-n}(H_2O)_n]^{(4-n)-}$ centers than in $[Fe^{II}(CN)_6]^{4-}$ centers, as shown in step 3a. In step 4a, a $[Fe^{III}(CN)_{6-n}(H_2O)_n]^{(3-n)-}$ unit reacts with undissociated Fe(II)−Pt(IV)−Fe(II) to yield a form of PB▼.

The proposed photochemical mechanism of PB▼ formation is similar to the dark mechanism. In step 1b, the absorption of light into the Fe(II) → Pt(IV) IT band of Fe(II)−Pt(IV)−Fe(II) results in the dissociation of the complex into $Fe(CN)_6^{3-}$ and $Pt(NH_3)_4^{2+}$. In step 2b, H^+ ions undergo hydrogen bonding to terminal cyanide ligands of $Fe(CN)_6^{3-}$, weakening the $Fe(t_{2g})$ to $CN(\pi^*)$ back-bonding and facilitating cyanide loss. In general, $Fe(t_{2g})$ to $CN(\pi^*)$ back-bonding is weaker in Fe(III) centers than in Fe(II) centers; therefore, cyanide loss through this mechanism (step 3b) should be more favorable from $Fe^{III}(CN)_6^{3-}$ than from $Fe^{II}(CN)_6^{4-}$ centers. Following ligand loss, the resulting $[Fe^{III}(CN)_{6-n}(H_2O)_n]^{(3-n)-}$ unit reacts with undissociated Fe(II)−Pt(IV)−Fe(II) to yield a form of PB▼, as shown in step 4b. Because $Fe(CN)_6^{3-}$ is photolabile,[21,22] a second photochemical pathway to PB▼ exists. Step 2c shows photoinduced cyanide loss from $Fe(CN)_6^{3-}$. The resulting $[Fe^{III}(CN)_5(H_2O)]^{2-}$ reacts with undissociated Fe(II)−Pt(IV)−Fe(II) to yield a form of PB▼, as shown in step 3c. The proposed photochemical mechanism accounts for the significantly faster formation of PB▼ in irradiated samples than in nonirradiated samples. The rate of Fe(II) oxidation is dramatically increased with photochemical oxidation to $Fe(CN)_6^{3-}$ through dissociation of Fe(II)−Pt(IV)−Fe(II). In addition, the rate of cyanide loss is increased through photolabilization of $Fe(CN)_6^{3-}$. Thus, the overall mechanism outlined in Scheme 1 is consistent with the relative rates of PB▼ formation in irradiated and nonirradiated samples, as well as the experimentally observed dependence of PB▼ formation on H^+, Pd^{2+}, and O_2.

The proposed mechanism may apply equally well to the acid-catalyzed formation of PB from $Fe(CN)_6$.[4−] It is well-known that $Fe(CN)_6^{4-}$ is oxidized to PB in acidic aqueous solution.[26] However, little has been written about the exact mechanism of this process. We believe that the proposed mechanism of coupled acid-catalyzed cyanide loss and Fe(II) oxidation provides a reasonable pathway for acid-catalyzed PB formation from $Fe(CN)_6^{4-}$.

Photochemical Image Generation. The [Fe(II)−Pt(IV)−Fe(II)]−[$PdCl_4^{2-}$] cyanogel system enables a novel approach to photochemical image generation. Because of the polymeric nature of the cyanogel system, a vast number of PB▼ photoproducts are possible, differing in the number of Fe(II)−Pt(IV)−Fe(II) subunits, the number of Pd(II) linkages, and the number of Fe(III) linkages. All PB▼ species should undergo Fe(II) → Fe(III) IT at significantly lower energy than the Fe(II) → Pt(IV) and Fe(II) → Pd(II) IT processes which occur in the nonirradiated gel. The energy difference between the charge-transfer processes occurring in the irradiated and nonirradiated regions of the sample enables arbitrary image generation.

The production of a series of diffraction gratings was chosen as a simple demonstration of the image generation potential of the [Fe(II)−Pt(IV)−Fe(II)]−[$PdCl_4^{2-}$] cyanogel system. Samples in 0.12 cm path length photochemical cells were irradiated at 488.0 nm with an expanded beam through a diffraction grating mask consisting of four patterns with repeat distances (d) ranging from 47 to 98 μm, as shown in Figure 7a. Figure 7b shows a photograph of an irradiated gel sample at 65× magnification. The negative images of the four patterns from the mask are clearly transferred to the cyanogel sample. The darker areas correspond to the irradiated regions of the sample which are actually green because of PB▼ formation. The lighter areas of the sample correspond to the masked, nonirradiated regions of the sample which are actually orange. In these regions, the Fe(II) → Pt(IV) and Fe(II) → Pd(II) IT absorptions remain intact, and no Fe(II) → Fe(III) band has formed. The image produced is the negative of the mask, because the irradiated areas turn dark while the nonirradiated areas remain light-colored.

Because the green regions of the sample absorb red light and the orange regions do not, a diffraction pattern is generated when red light is shone through the samples. Figure 7c shows the diffraction of 680 nm light by the four regions of the sample. The diffraction patterns correspond very accurately with those from the diffraction gratings on the mask. The diffraction pattern results from Fraunhofer diffraction (eq 1), where n is the order of diffraction, λ is the wavelength of incident light, d is the spacing between rows in the diffraction grating, and ϕ is the angle between the

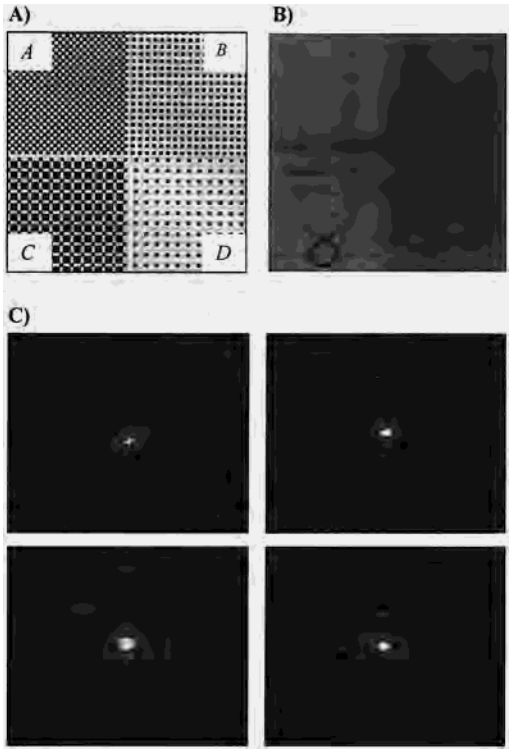

Figure 7. (A) Patterns of irradiation mask. (B) Photochemically patterned [Fe(II)−Pt(IV)−Fe(II)]−[$PdCl_4^{2-}$] cyanogel sample (magnified 65×) following 488 nm irradiation through the mask shown in (A). The line in the lower left region of the sample corresponds to a 200 μm distance. The circle indicates a region of dark coloration in the cyanogel sample which has no corresponding white region in the mask. (C) Patterns resulting from diffraction of 680 nm light by the four regions of the cyanogel sample in (A).

Table 1. Comparison of Photochemically Produced Diffraction Gratings in a [Fe(II)−Pt(IV)−Fe(II)]−[$PdCl_4^{2-}$] Cyanogel Sample with the Corresponding Gratings in the Mask

pattern	ϕ mask (rad)	ϕ cyanogel (rad)	d mask[a] (μm)	d cyanogel[a] (μm)	R cyanogel[b] (μm)
A	0.014	0.014	47	47	24
B	0.010	0.010	67	67	12
C	0.0069	0.0069	98	98	17
D	0.0074	0.0069	92	98	17

[a] Values of d were calculated on the basis of the measured values of ϕ using eq 1, where $\lambda = 680$ nm and n=1 (first-order diffraction distances measured in the calculation of ϕ). [b] R = resolution of pattern. $R = d/2$ in pattern A and $d/6$ in patterns B, C, and D (see text).

directions of incident and scattered light.

$$n\lambda = d \sin \phi \qquad (1)$$

Using the Fraunhofer diffraction equation, the values of d for the [Fe(II)−Pt(IV)−Fe(II)]−[$PdCl_4^{2-}$] cyanogel diffraction gratings and the mask diffraction gratings were calculated and compared (Table 1). The calculated values of d for the cyanogel matched those of the mask very closely.

In a separate experiment, a lined diffraction grating was produced in a cyanogel sample. The lined grating gives rise to a one-dimensional diffraction pattern. Diffraction to the 11th order was detectable with a silicon photodiode. The log of light intensity (I) as a function of diffraction angle (ϕ in eq 1) is shown in Figure 8 for the first 8 orders of diffraction ($n = 1-8$ in eq 1). The spacing (d in eq 1) of

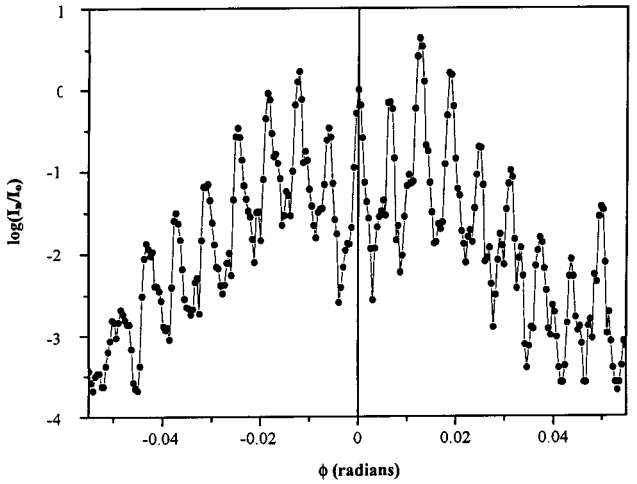

Figure 8. Plot of $\log(I_n/I_0)$ vs ϕ, where I_n is the intensity of the nth-order diffracted light, I_0 is the intensity of the nondiffracted (zeroth-order) light, and ϕ is the angle between the nth-order and zeroth-order beams, for diffraction of 633 nm light through a lined diffraction grating photochemically printed in a cyanogel sample. On the basis of the maxima in the plot, the spacing in the diffraction grating was calculated to be 102 ± 1.7 μm.

Table 2. Measured Diffraction Efficiencies for Diffraction of 633 nm Light by Lined Cyanogel Fraunhofer Grating with 102 ± 1.7 μm Line Spacing

diffraction order, n	diffraction efficiency, DE[a] (%)
−8	0.01
−7	0.06
−6	0.14
−5	0.30
−4	1.56
−3	4.18
−2	7.69
−1	1.55
0	4.59
1	3.25
2	19.95
3	7.33
4	0.89
5	0.47
6	0.07
7	0.04
8	0.17

[a] DE = (I_n/I_{inc}), where I_n is the intensity of light in the nth order of diffraction and I_{inc} is the intensity of light incident on the diffraction grating.

both the diffraction grating and the mask used to produce it were calculated from the experimentally measured values of ϕ at the maxima of log I versus ϕ plots. The spacing of the diffraction grating was calculated to be 102 ± 1.7 μm, while the spacing of the mask used to produce the grating was calculated to be 104 ± 1.4 μm. Thus, the grating in the cyanogel sample is a very accurate reproduction of the grating in the mask. The diffraction efficiencies for each order of diffraction in the cyanogel grating are shown in Table 2. The sum of diffraction efficiencies is less than 100% because of Rayleigh scattering of light from the colloidal particles of the sol−gel sample, which is unrelated to the quality of the optical pattern in the gel.

Close inspection of Figure 7b reveals that the diffraction gratings generated in the cyanogel sample contain features not found in the diffraction gratings of the irradiation mask (Figure 7a). The patterns generated by irradiation through

regions *B*, *C*, and *D* of the mask contain additional areas of $PB^{\blacktriangledown}$ which do not correspond to a clear area in the irradiation mask. (See, for instance, the circled area in region *C* of the cyanogel photograph. These features were much clearer when viewed directly through the microscope but did not photograph well.) The circled area in region *C* highlights a green spot ($PB^{\blacktriangledown}$) in the center of an orange region (undissociated Fe(II)−Pt(IV)−Fe(II)). The corresponding area of the irradiation mask contains only a black region. The difference between the mask and cyanogel images results from the diffraction of 488 nm light passing through the multiple slit grating of the mask. The pattern formed in the cyanogel sample actually corresponds to the interference pattern of the 488 nm light and thus contains features not present in the mask. When the spacing in the pattern of the mask is small enough, the photochemically generated pattern in the cyanogel sample has a smaller repeat distance than the pattern of the mask itself.

In general, the resolution of a pattern is equal to the size of its smallest feature, or half the repeat distance, *d*. However, in patterns *B*, *C*, and *D*, the resolution is less than half the calculated repeat distance, because of the presence of additional features within the pattern. Within one-half the measured repeat distance, *d*, these patterns contain alternating regions of (1) undissociated Fe(II)−Pt(IV)−Fe(II), (2) $PB^{\blacktriangledown}$, and (3) undissociated Fe(II)−Pt(IV)−Fe(II). Therefore, the maximum resolution of patterns *B*, *C*, and *D* must be one-sixth the measured repeat distance. The resolution of each pattern within the cyanogel sample is shown in Table 1. The highest resolution measured was 12 μm in pattern *B*.

Conclusions

The [Fe(II)−Pt(IV)−Fe(II)]−[$PdCl_4^{2-}$] cyanogel system has been described. Irradiation into the Fe(II) → Pt(IV) IT band causes the formation of a variety of $PB^{\blacktriangledown}$ species through photochemical and dark pathways. An overall mechanism of $PB^{\blacktriangledown}$ formation involving coupled cyanide loss and Fe(II) oxidation has been proposed. The mechanism is consistent with the observed influence of H^+, Pd^{2+}, and O_2 on $PB^{\blacktriangledown}$ formation. It has also been noted that this mechanism may account for the formation of PB from $Fe(CN)_6^{4-}$ in acidic aqueous solution. The image generation potential of this system was demonstrated by the production of a series of Fraunhofer diffraction gratings with features on the order of 12 μm. Eleven orders of diffraction were detected from the gratings.

To the best of our knowledge, the cyanogel system is the first reported example of an octahedral, transition-metal based sol−gel network capable of photochemical patterning. Optical processing of the [Fe(II)−Pt(IV)−Fe(II)]−[$PdCl_4^{2-}$] system is fundamentally different from that of modified silica and titania systems in which UV light is used to alter the surface structure of the sample. In the cyanogel system, pattern formation results from Fraunhofer diffraction through the optically contrasting irradiated and nonirradiated regions of the gel, rather than from Bragg diffraction from regions of photoinduced morphological changes. In addition, because the dissociative photochemistry of Fe(II)−Pt(IV)−Fe(II) occurs in the visible, photochemical image generation is possible with visible rather than UV irradiation. Furthermore, image generation occurs in one photochemical step, and no postphotochemical washing is required. The cyanogel system also differs from those in which a photoactive species is encapsulated in a photochemically inert sol−gel matrix. In the cyanogel system, the molecular component responsible for the structural rigidity of the sol−gel matrix is also the photochemically active portion of the system. The [Fe(II)−Pt(IV)−Fe(II)]−[$PdCl_4^{2-}$] system is unique among photoactive sol−gel systems with regard to its structure and photochemical mechanism. The ability to photochemically pattern a cyanogel system using visible light has potential applications in information storage, particularly in light of the system's inherent flexibility of sample size, shape, and volume.

Acknowledgment. The authors thank Prof. T. G. Spiro for the use of his Raman instrumentation. This work was supported by the National Science Foundation, under Grant CHE-0079169.

IC010710L